Phosphorylation sites are evolutionary checkpoints against liquid-solid transition in protein condensates

Srivastav Ranganathan[1]*, Pouria Dasmeh[2]*, Seth Furniss[1,3], and Eugene Shakhnovich[1]

shakhnovich@chemistry.harvard.edu

[1]Department of Chemistry and Chemical Biology, Harvard University, Cambridge, MA 02138

[2]Center for Human Genetics, Marburg University, Germany.

[3]Physical and Theoretical Chemistry Laboratory, Department of Chemistry. University of Oxford, South Parks Road, Oxford OX1 3QZ, United Kingdom

[*]These authors equally contributed to the work

Abstract. Assemblies of multivalent RNA-binding protein FUS can exist in the functional liquid-like state as well as less dynamic and potentially toxic amyloid- and hydrogel-like states. How could then cells form liquid-like condensates while avoiding their transformation to amyloids? Here we show how post-translational phosphorylation can provide a "handle" that prevents liquid-solid transition of intracellular condensates containing FUS. Using residue-specific coarse-grained simulations, for 85 different mammalian FUS sequences, we show how the number of phosphorylation sites and their spatial arrangement affect intracluster dynamics preventing conversion to amyloids. All atom simulations further confirm that phosphorylation can effectively reduce the β-sheet propensity in amyloid-prone fragments of FUS. A detailed evolutionary analysis shows that mammalian FUS PLDs are enriched in amyloid-prone stretches compared to control neutrally evolved sequences suggesting that mammalian FUS proteins evolved to self-assemble. However, in mammalian sequences phosphosites are often placed in close proximity to these amyloid-prone regions. These results suggest that evolution uses amyloid-prone sequences to enhance phase-separation of condensate proteins while enriching phosphorylation sites in close proximity to safe-guard against liquid-solid transitions.

Significance Statement.

Intrinsically disordered regions and prion-like domains are widely observed in proteins that get enriched in membrane-less organelles (MLOs). Mammalian Fused in Sarcoma (FUS) sequences are significantly enriched in amyloid-prone sequences suggesting that they have evolved to self-assemble. While the amyloid-prone stretches promote self-assembly of these proteins at lower threshold concentrations, these assemblies are vulnerable to aberrant liquid-solid phase transitions. Molecular simulations and bioinformatics analyses show that evolution overcomes this challenge by placing phosphosites specifically close to amyloid-prone stretches. Introduction of negatively charged residues at phosphosite locations results in fewer amyloid-prone contacts and thereby lower beta-sheet propensity. Phosphorylation can thus allow cells to utilize amyloid-prone stretches to promote biogenesis of MLOs while protecting against liquid-solid transitions.

Introduction

Biomolecular phase transitions is a universal mechanism of formation of "membraneless organelles" (MLOs) in mammalian cells. These organelles have been associated with diverse functions ranging from stress response to gene regulation [1–4]. A candidae physical mechanism to explain the formation of MLOs is intracellular liquid-liquid phase separation (LLPS) wherein inter-molecular interactions result in formation of a biopolymer-rich phase that is distinct from the bulk solution [1,5]. A key feature of proteins that engage in intracellular condensates is multivalency – the ability to participate in several adhesive interactions[6,7].

The role of multivalency in promoting phase separation is well established in model experimental and computational studies[6,7]. Multivalency can take different forms, including folded domains capable of specific protein-protein interactions in modular proteins, or low-complexity, intrinsically disordered regions that can participate in multiple attractive inter-protein interactions[1,3]. Over the past decade, intrinsically disordered regions (IDRs) have been identified to be widely prevalent in phase-separating proteins[8,9]. The multivalent interactions involving these regions has been found to reduce threshold concentrations for phase-separation of folded domains by an order of magnitude[10].

A subset of these intrinsically disordered domains are the low-complexity, prion-like domains enriched in a select subset of amino acids – Asn (N), Gln (Q), Tyr (Y), Ser (S) and Gly (G)[11]. The composition of these prion-like domains is reminiscent of self-replicating amyloidogenic segments in yeast prion proteins such as Sup35 and Ure2[12,13]. This suggests an interesting paradox. While the multivalency of IDRs stems from their ability to participate in diverse interactions (pi-pi/cation, hydrophobic, electrostatics) and thus allows LLPS to occur at physiological concentrations, a high density of prion-like domains (PLDs) within the condensed phase makes these structures prone to detrimental, liquid-solid phase transitions. Indeed, PLDs of RNA-binding domains have been observed to populate diverse physical states such as liquid-droplets, hydrogels and ordered amyloid-like structures[11,14,15]. Full-length FUS proteins that initially self-assemble into dynamic, liquid-like droplets over time evolve into amyloid-like solid structures in a process known as maturation of droplets in vitro[15]. These results suggest that the amyloid-like state could potentially be an equilibrium configuration for IDR-rich phase-separated structures.

How then cells strike a balance between the functional role of IDRs (ability to phase

separate) and their deleterious effects (irreversible liquid-solid transitions) is an open question. In this context, active mechanisms such as post-translational modifications may play an important role in preventing liquid-solid transitions in the cell[16]. Phosphorylation, methylation, acetylation and ribosylation have all been reported in intrinsically disordered regions of phase-separating proteins[17.] For example, Monahan et al demonstrated that phosphomimics of FUS have a lower propensity to undergo liquid-solid transitions[18]. Other studies have also shown that the FUS PLD can have up to 31 phosphorylation sites spread across the length of the domain. Bioinformatics analysis have shown that primate FUS PLD sequences also harbor the highest number of potential phosphosites, with a three-fold higher probability of phosphosite-creating substitutions, compared to other species[19]. These observations suggest that phosphrylation may act as a handle that tunes phase separation. However, mechanistic understanding of the role of phosphorylation as a handle tuning phase separation has been lacking.

We employ a residue-specific coarse-grained model for FUS as well as all atom simulations and evolutionary analysis to study how phosphorylation influences the inter-protein interaction network as well as intracluster dynamics in phase-separated FUS proteins. Using a residue-specific coarse-grained model proposed by Dignon et al[20], we show how intracluster dynamics of FUS PLD assemblies is primarily mediated by Tyrosine and Glutamine residues. We further study the effect of phosphorylation on phase behavior of condensates by systematically varying the extent of phosphorylation as well as generating different phosphorylation patterns. Our results show that phosphorylation results in a switch in the predominant interaction network to heterodomain interactions, for full-length FUS assemblies. Importantly, we show that the intracluster dynamics, and diffusion coefficients are not only sensitive to the net charge of the FUS prion-like domain but also the location of the modification sites. All atom simulations further support the role of phosphorylation in drastically diminishing the propensity of amyloid-rich fragments of FUS sequences to form aberrant beta structure. Using simulations and bioinformatics analysis with 85-different mammalian FUS sequences, we also show that the number, and location of phosphosites are strongly correlated with the overall amyloidigenic propensity of a sequence, and, more specifically phosphorylation sites appear to be preferentially located near amyloid-rich segments of FUS proteins. Overall, our study shows that phosphorylation sites in IDRs likely serve as evolutionary checkpoints against solidification via amyloid-like transitions.

Model

Coarse-grained semi-flexible polymer model for FUS.

We performed Langevin dynamics simulations using a semi-flexible polymer representation of FUS wherein we model the protein at residue level details. We employ a coarse-grained framework previously developed by Dignon et al. for simulating phase-separation of proteins such as LAF1 and the low complexity domain of FUS[20]. Here, each amino-acid is modeled as a single bead in a bead-spring polymer with the physicochemical properties of the bead (hydrophobicity, charge) being mapped onto one of 20 naturally occuring amino acids. To model inter- and intra-chain protein-protein interactions, we employ a hydrophobicity-based interaction potential used by Dignon et al. to study LAF1 phase separation[20], and first described by Ashbaugh and Hatch[21]. This approach, refered to as the hydrophobicity scale (HPS) method, uses the hydrophobicity scale to define interacions betweena amino acids. The hydrophobicity values for the coarse-grained amino acid beads are scaled from 0 to 1 (with 1 being the most hydrophobic amino acid.) The net hydrophobic strength of an interaction between two coarse-grained amino acids is the arithmetic mean of their individual hydrophobicities (Supplementary Table.1). The Ashbaugh-Hatch potential describing interaction between coarse-grained amino acids assumes the form[20],

$$E(r) = \begin{cases} E_{nb} + (1 - H_{ij})\epsilon_{aa}, & \text{if } |ri - rj| <= 2^{1/6}\sigma \\ H_{ij} * E_{nb}, & \text{otherwise} \end{cases} \quad (1)$$

and

$$E_{nb} = 4\epsilon \sum_{i<j} \left[\left(\frac{\sigma}{|\vec{r}_i - \vec{r}_j|} \right)^{12} - \left(\frac{\sigma}{|\vec{r}_i - \vec{r}_j|} \right)^{6} \right] \quad (2)$$

for all $|\vec{r}_i - \vec{r}_j| < r_c$. Here r_c refers to the interaction cutoff beyond which LJ interactions are neglected. The cutoff for LJ calculations were set to 2.5 times of σ. Here, H refers to the net hydrophobicity of an interacting amino-acid pair which is the arithmetic mean of their individual hydrophobicities while ϵ_{aa} is the strength of the attractive interaction which gets scaled depending on the properties of the amino acid. ϵ_{aa} was set to 0.2 kcal/mol, a value which resulted in experimentally comparable values for radius of gyration values of intrinsically disordered proteins in the study by Dignon et al[20]. In order to model phosphomimetic FUS sequences, we substitute the phosphosite S/T residues to Glutamic acid (S/T -> E), introducing a negative charge at the site. Similar approach to study phosphorylation of the FUS prion-like domain has been adopted by Perdikari et al[22] in their simulation study and Monahan et al in vitro[18].

Methods

Coarse-grained simulations.

Peptides/proteins have been extensively modeled at coarse-grained resolution to study biomolecular structure and self-assembly[6,23–26]. Fewer degrees of freedom in coarse-grained polymers leads to higher computational tractability, making them efficient tools to study biomolecular phase transitions[25,27–32]. In order to study the effect of phosphorylation on LLPS of FUS and the resultant intra-cluster dynamics, we performed Langevin dynamics simulations. To simulate self-assembly, we perform simulations with 50 coarse-grained FUS (full-length or PLD) chains in a cubic box with periodic boundaries enabled.

Coarse-grained FUS polymer beads interact via the following bonded and non-bonded potential functions. Adjacent beads in a polymer chain are bonded via the harmonic potential with energy

$$E_{stretch} = k_s \sum_{i=1}^{M-1} (|\vec{r}_i - \vec{r}_{i+1}| - r_0)^2, \quad (3)$$

where $\vec{r}_i$ and $\vec{r}_{i+1}$ correspond to the positions of the i^{th} and $(i+1)^{th}$ beads, respectively; r_0 is the resting bond length. k_s denotes the spring constant and has units of kT/Å^2. This interaction ensures the connectivity between the adjacent beads of the same polymer chain. For the coarse-grained FUS polymers, we use a k_s of 2 kT//Å^2.

To model the semi-flexible nature of the self-assembling intrinsically disordered proteins, neighboring bonds in a polymer chain interact via a bending potential

$$E_{bend} = \kappa \sum_{i=1}^{M-2} (1 - cos\ \theta_i), \quad (4)$$

where θ_i refers to the angle between i^{th} and $(i+1)^{th}$ bond. Here, κ the bending stiffness, has units energy, kT. We employ a κ of 4 kT or equivalently, a persistence length of roughly 5 polymer beads (or 5 amino acid residues). The contour length of the FUS prion-like domain, in comparision is 165 residues long.

Pairwise non-bonded interactions were modeled using a combination of Lennard-jones and Ashbaugh and Hatch potential (see Model section for details). Screened electrostatic interactions were modeled using the Debye-Huckel electrostatic potential,

$$E_{DH} = \frac{q_i q_j}{4\pi.Dr}.exp\frac{-r}{\kappa} \quad (5)$$

Here, q_i and q_j are the charges of the two coarse-grained amino acid beads (Table S1). This

approach has been previously employed in phase separation simulations by Dignon et al.[22,23,33]and can recapitulate behavior of intrinsically disordered proteins such as TDP43 and FUS. The Debye-Huckel screening length of 1 nm was employed in our coarse-grained simulations to mimic the screening of electrostatic interactions in a cellular environment.

The LAMMPS molecular dynamics package was employed to perform the coarse-grained Langevin dynamics simulations[34]. Here, the simulator solves Newton's equations in presence of a viscous force while the Langevin thermostat is used to implement the NVT ensemble with a simulation temperature of 310 K. An integration timestep (dt) of 15 fs was used for the simulations.

Simulation protocol – coarse-grained simulations.

To ensure efficient sampling of the self-assembly landscape, and to access a single large spherical condensate at simulation timescales, we employed metadynamics simulations[35]. In these history-dependent metadynamics simulations, energy gaussians are deposited during the course of the simulation along a reaction coordinate that describes self-assembly. Here, the reaction coordinate along which the metadynamics simulation is performed is the radius of gyration of an imaginary polymer -- R_g^{system} -- that is composed of the 50 center of masses corresponding to the constituent polymer chains in the system. In Supplementary Fig.S1, we show the free energy profile of a system of 100 FUS chains at an effective concentration of 100 uM. Values of R^g_{system} approaching 150 Angstroms corresponds to a single large spherical condensate while at higher values (> 200 Angstroms), the system approaches the fully mixed state. As evident from the free-energy profile, the system of FUS proteins favors the demixed, self-assembled state. This configuration corresponding to the single large assembly (the free energy minima in metadynamics simulations) was then used as a starting configuration for conventional Langevin dynamics trajectories (with no biasing potential) of at least 10 microseconds or till the simulations reached convergence. These unbiased 10-microsecond long simulation trajectories were used to compute statistical quantities (inter-protein contacts, diffusion coefficients) in this paper.

All-atom molecular dynamics.

To study secondary structural propensity of amyloidogenic peptides derived from the FUS prion-like domain (PLD), we employed atomistic molecular dynamics simulations. To study the β-sheet

propensity of the FUS PLD-derived peptides and the role of phosphorylation in abrogating inter-peptide β-sheet formation, we performed metadynamics simulations with 50 molecules of peptides derived from $FUS_{1\text{-}165}$ and their phosphomimetic counterparts (see Supplementary Table. S4 for sequences). The radius of gyration of the system of 50 peptides (R_g^{system}) was used as a reaction coordinate along which the metadynamics[35] simulations were performed. The structures corresponding to the free energy minima in metadynamics simulations were used to analyze secondary structural propensity of the peptides. The simulations were performed using the NAMD[36] molecular dynamics package with an electrostatic cutoff of 12 Å units and a van der Waals cutoff of 10 Å units along with periodic boundary conditions. The systems were first energy-minimized and then heated to 310 K with a gradual scaled increase in temperature. This was followed by a constant pressure equilibration for 5 ns and then an NPT (isothermal-isobaric ensemble) production run. The CHARMM36 protein forcefield[37], and the TIP3P water model was used to simulate proteins at atomistic resolution. All simulations were performed until the simulations reached convergence.

Simulation of neutrally evolved sequences

We employed the Evolver package within the PAML suite[38] to simulate protein evolution. This approach uses Monte Carlo simulations to generate codon sequences using a specified phylogenetic tree with given branch lengths, nucleotide frequencies, transition/transversion bias, and the ratio of the rate of nonsynonymous to synonymous substitutions (dN/dS; [39]). For neutral sequence evolution, we used the standard genetic code with codon frequencies taken from mammalian FUS sequences. In the simulations, we assumed a protein length of 600 codons but reported our measured quantities per 100 amino acids to account for different lengths of mammalian PLD sequences and our simulated sequences. We used a consensus phylogenetic tree for the mammalian from the TimeTree database ([40]). In our phylogenetic trees, the branch lengths represent the expected number of nucleotide substitutions per codons. To model neutral evolution, we set d*N*/d*S* to 1 and used a transition/transversion rate ratio of 4.09 which we estimated from the PLD sequence of FUS orthologs. We estimated these values by fitting the codon model M1 to the phylogenetic tree and the sequences of these proteins[41]. This model assumes that all branches of the phylogenetic tree have the same rate of evolution.

Nomenclature. The 526-residue long FUS protein will be referred to as the full-length FUS. The FUS prion-like domain, on the other hand, will hereby be referred to as $FUS_{1\text{-}165}$.

Results

Tyrosine and Glutamine contacts are modulators of intracluster dynamics

The FUS family of proteins, including the FUS itself , feature a multi-domain architecture with a low complexity prion-like domain, an RNA-recognition motif and an arginine rich C-terminal domain[11]]. Previous studies have extensively established the different interaction networks and the hierarchy of interactions stabilizing the liquid-like FUS condensate[11]. The PLDs of FUS are also known to self-assemble into hydrogels and solid-like structures[14]. Given the association between interaction networks and the material state of the condensate, it becomes critical to understand the interactions stabilizing the condensed phase.

To identify the key 'sticky' interactions in the PLD, we performed simulations with 165-residue long coarse-grained peptide chains (same as the length of the PLD) of the following sequences - i) $polyG_{165}$,ii) $polyY_{165}$, iii) $polyST_{165}$, iv) $FUS_{1\text{-}165}$ – hereby referred to as $FUS_{1\text{-}165}$, v) $FUS_{1\text{-}165}$ with Glycines replaced by Glutamines (G->Q), vi) $FUS_{1\text{-}165}$ with glycines substituted with serine (G->S) and vii) sequences where serine or glutamine residues are replaced by glycines (S>G and Q>G). These substitutions were performed on the 4 most abundant residue types in $FUS_{1\text{-}165}$ -- G/Q/S/Y (Fig.1A). Using the coarse-grained forcefield for phase-separating proteins first developed by Dignon et al [33], we first perform metadynamics (see methods) simulations to enable the formation of the condensed phase within simulation timescales. We subsequently run long trajectories (10 μs) to analyze the interaction networks within protein clusters. As shown in Fig.1B, the polyG chains remain in a monomeric state and develop negligible interpeptide contacts. polyY, chains on the other hand show the strongest interpeptide contact development within the condensed phase. polyST sequences form self-assembled structures with sparser inter-molecular interactions than polyY chains. The native PLD sequence, on the other hand, shows an intermediate level of inter-peptide contacts, sparser than polyY chains and stronger than polyST chains. Interestingly, modifying the glycine residues in the FUS PLD to glutamine and serine does'nt result in a significant increase in interpeptide contacts. However, mutating the glycine

residues of the FUS PLD to either Glutamine or Serine (G->S and G->Q in Fig.1C) results in a dramatic slowdown in intracluster environments. Conversely, modifying S/Q -> G results in assemblies that are more dynamic than the FUS_{1-165} assemblies (Fig. 1B). Interestingly, G->S and S->G substitutions are the most frequent substitutions among mammalian FUS orthologs[42]. These results show that while Tyrosine residues are the strongest drivers of phase-separation in the FUS PLD (Fig. 1A), the intracluster dynamics within the dense phase depends significantly on inter-peptide contacts involving Tyr and Gln (purple and black curves in Fig.1C). These results are consistent with experiments and simulations studying FUS interaction network[11,15,20] suggesting that the coarse-grained model can robustly capture features of FUS phase separation. Simulations with homopolymer and amino-acid substituted sequences also suggest that interpeptide contacts involving Tyr and Gln could be robust predictors of intra-cluster dynamics.

Upon identifying how interactions involving the 4 most-abundant amino acids in the FUS PLD can modulate the intracluster dynamics within protein assemblies, we study whether (and how) shuffling of the PLD sequence in full-length FUS protein could tune the interaction network within the FUS condensates. To understand the key contacts that stabilize the assembly, we randomize the sequence of the FUS PLD (residues 1-165), keeping the amino acid composition of the PLD intact (Supplementary Fig.S2A) and the RNA-binding domain (RBD) sequence unchanged. We observed that shuffling of the PLD sequence results in an almost 2-fold variation in the number of PLD-PLD contacts within the condensed phase (Supplementary Fig.S2B). Crucially, the number of PLD-PLD contacts in shuffled sequences is strongly correlated with number of interactions involving Tyrosine and Glutamine residues in the PLD (Supplementary Fig.S2C and D). However, an increase in Tyr and Gln contacts does not lead to an increase in contacts involving Ser and Gly (Supplementary Fig.S3), the other two most abundant residues in the PLD of FUS (Supplementary Fig.2A), suggesting that the density of the PLD-PLD interactions is primarily modulated by the Tyrosine and Glutamine residues.

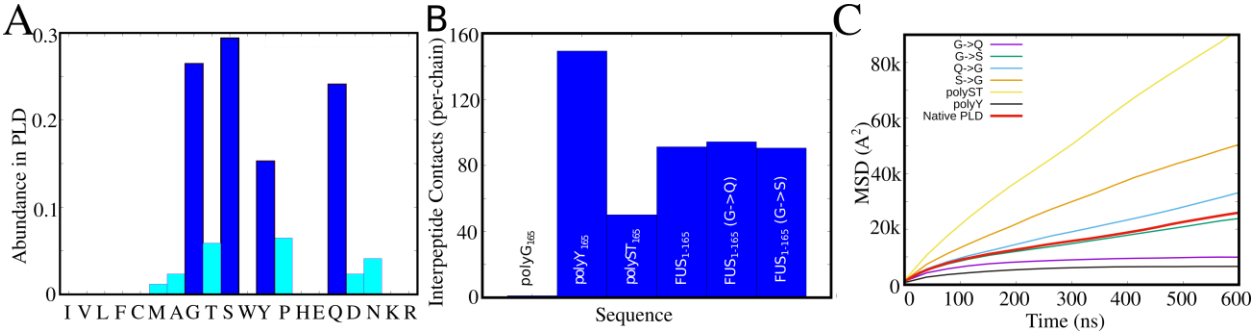

Figure 1: Identifying spacers and stickers in FUS prion-like domain. A) Amino acid residues and their abundances in the FUS PLD B) Comparison of inter-peptide contacts (per chain) for different 165-residue long peptide chains. $polyG_{165}$ chains remain in the monomeric state. polyY chains show the highest inter-peptide interaction propensity while polyST sequences show an intermediate degree of interaction. The native FUS PLD clusters show inter-peptide contacts sparser than polyY clusters but greater than polyST clusters. C) The mean-square displacement profiles for different 165-residue long peptides. polyST sequences form self-assembled clusters that are more liquid-like than polyY and native FUS PLD clusters. polyY clusters are the most solid-like among all sequences studied. Mutations to glycine residues (G->S and G->Q) results in a slowdown in intracluster dynamics. On the other hand, mutating S/Q -> G results in a more dynamic intracluster environment than the native FUS PLD sequence.

Phosphorylation reduces the likelihood of PLD-PLD contacts while the PLD-RBD interactions remain unaffected

The coarse-grained model can capture the known features of FUS interaction networks where Gly/Ser are spacers and Tyr/Gln are stickers thereby making it suitable to study the role of phosphorylation on the FUS condensate interaction network **(Fig 1 and S1)**. In order to model phosphorylated FUS sequences, we replace the S/T residues at phosphosites to Glutamic acid (S/T -> E), thereby introducing a negative charge at the site. The human FUS PLD sequence has 31 potential phosphosites[19] (Supplementary Table S2 and S3). We systematically vary the fraction of phosphosites **(P_{frac})** that are modified, and also simulated different phosphorylation patterns for each modification fraction. As we increase the fraction of phosphosites that are modified -- **(P_{frac})** --, we observe an increased likelihood of the heterodomain interactions (Fig. 2A). For **$P_{frac} \rightarrow 0$,** the PLDs are equally likely to participate in homodomain (with other PLDs) or heterodomain interactions (with RBDs of other molecules). On the other hand, as **$P_{frac} \rightarrow 0.9$**, we see a 2-fold higher likelihood of PLD-RBD interactions as compared to the PLD-PLD interactions.

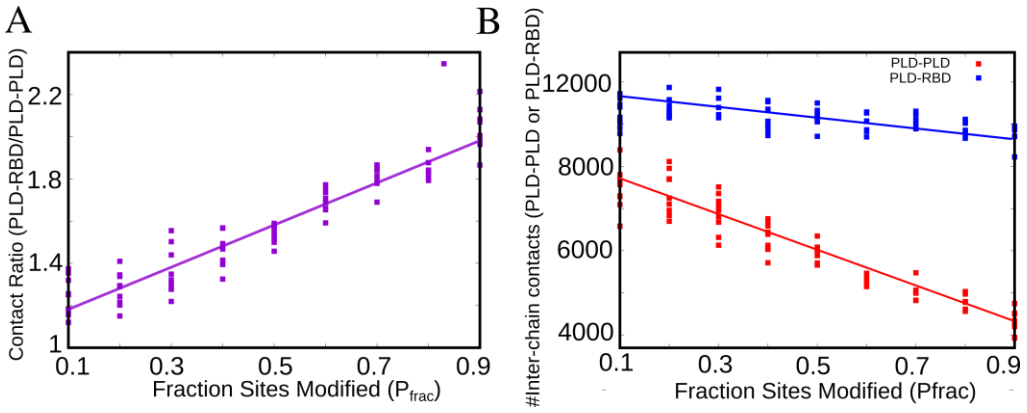

Figure 2: Network switching in full-length FUS as a result of Phosphorylation. A) The ratio of inter-peptide PLD-RBD to PLD-PLD contacts within the self-assembled cluster as a function of varying modification fraction– fraction of residues modified out of a potential 31 phosphosites. B) The effect of

phosphorylation on PLD-PLD and PLD-RBD interaction network. Each point in the figure corresponds to a different modification pattern, for a given fraction of sites modified.

Further, we probed whether this switch in interaction networks is an outcome of reduced PLD-PLD interactions or increased PLD-RBD interactions. We find that an increase in modification fraction does not significantly alter the extent of interchain PLD-RBD interactions (Fig 2B, blue curve). On the other hand, the PLD-PLD interactions show a 2-fold decrease (Fig 2B, red curve) as we increase the modification fraction from 0.1 to 0.9 suggesting that phosphorylation can affect interaction networks by selectively modulating PLD-PLD interactions.

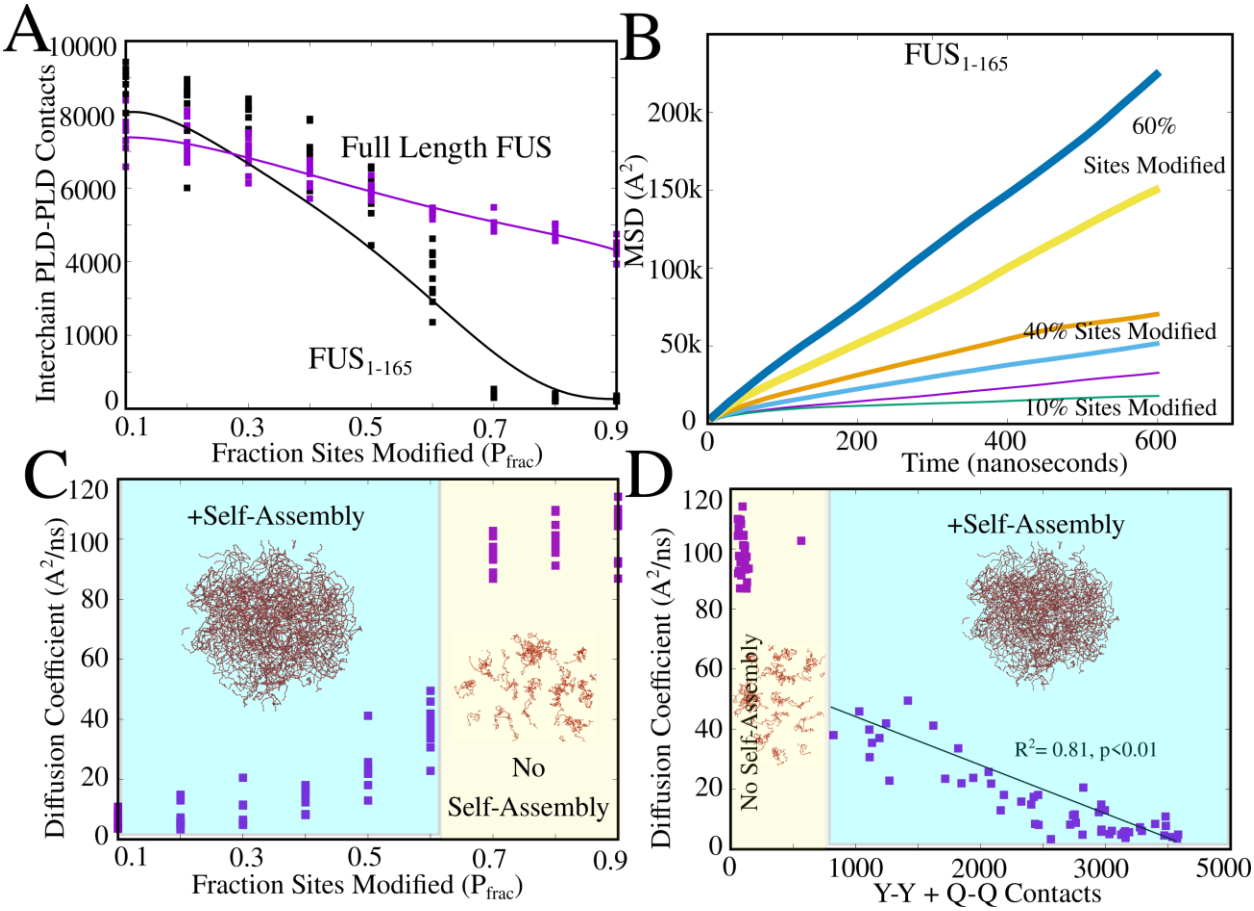

Figure 3: Phosphorylation tunes intracluster dynamics in FUS_{1-165} assemblies. A) PLD-PLD contacts as a function of increasing fraction of phosphosites modified. Purple curve corresponds to full-length FUS (PLD+RBD) while black curve shows results from FUS_{1-165} simulations. Each point corresponds to a different modification pattern, for any $\mathbf{P_{frac}}$. B) Representative mean-square displacement profiles for polymer chains within the FUS_{1-165} self-assembly. Higher the slope of the curve, more dynamic the intra-droplet environment. C) Diffusion coefficients within the FUS_{1-165} assembly (obtained by fitting MSD profiles to $MSD = 6 * D * t$. D) Diffusion coefficients are inversely correlated to the number of sticky interactions (Tyr-Tyr and Gln-Gln) within a cluster. +Self-assembly refers to the regime where the largest cluster sizes, $L_{clus} \rightarrow 1$, a single large cluster. In the -Self-assembly regime (shaded yellow), $L_{clus} << 1$ (see Supplementary Fig.S4 for cluster sizes).

Phosphorylation maintains liquid-like intracluster environment for PLD assemblies

The FUS PLD (FUS_{1-165}) has been observed to self-assemble into liquid-like droplets and undergo liquid-to-solid transitions in vitro[18,43]. Also, previous coarse-grained simulations have shown that disorder-order and liquid-solid transitions in FUS are characterized by homotypic contacts involving the PLD[26]. Our simulations with phosphorylated full-length FUS sequences establish that the introduction of negative charges in the PLD selectively tunes PLD-PLD interactions (Fig.2B). Therefore, the effect of phosphorylation can be effectively understood by studying FUS PLDs alone. Hereon, we switch to simulations of PLDs (FUS_{1-165} instead of the full-length protein), allowing for increased computational tractability of the simulations.

We first systematically vary the fraction of modified phosphosites, **(P_{frac}),** with different phosphorylation patterns for each fraction, and study the effect on the inter-molecular PLD-PLD contacts (Fig.3A). As with the full length FUS, we observe a decrease in PLD-PLD interactions at higher $\mathbf{P_{frac}}$. However, unlike the full-length protein, at $\mathbf{P_{frac}} > 0.6$ the PLD-peptides remain in monomeric state (Fig.3A, black curve and Supplementary Fig.S4). This is consistent with experiments which show that phosphorylation results in an increase in threshold concentrations for phase separation of PLDs [44]. The full-length protein, on the other hand, continues to remain in the phase-separated form even at high modification fractions, due to stabilization by heterodomain interactions (Fig.3A, purple curve). In Supplementary Fig.S4, we plot the size of the largest cluster size (L_{clus}) as a function of (P_{frac}). While full-length FUS remains in the self-assembled state throughout (L_{clus} -> 1), at $P_{frac} > 0.6$, the largest cluster size for FUS_{1-165} << 1. Hence, even at high modification fractions, the inter-peptide interactions for full-length FUS do not vanish unlike the PLD-only simulations with $FUS_{1-165\ chains}$ (Supplementary Fig. S4).

We further probe whether this reduced amount of PLD-PLD interactions at higher P_{frac} has an effect on intracluster dynamics of proteins. In Fig.3B, we plot the mean square displacement of polymer chains within the self-assembled cluster as a function of time. As we increase the extent of phosphorylation, the slope of MSD curves progressively increases suggesting more-liquid like behavior of phosphorylated PLDs. Interestingly, even for the same P_{frac}, we observe variability in MSD profiles (and inter-chain contacts) for different modification patterns. We further compute the diffusion exponents from the mean-square displacement profiles ($MSD = 6Dt$). The diffusion

coefficients corresponding to different modification fractions and patterns is shown in Fig. 3C. At lower $P_{frac,}$ the clusters are more likely to exhibit slow intracluster dynamics, as evident from the smaller values of the diffusion constants. As we increase the extent of phosphorylation, we see a concommitant increase in the diffusion coefficients suggesting more dynamic intra-cluster environment for these sequences. The diffusion coefficient is strongly correlated with the number of sticky contacts involving Tyr and Gln within the cluster (Fig.3B), consistent with experimental findings that show that stronger involvement of glutamines in inter-peptide interactions slows down intra-cluster dynamics[11]. Varying the extent of phosphorylation results in a 4-fold variation in diffusion coefficients within the self-assembled state (see region shaded blue in Fig. 3C). Overall, these findings suggest that the extent of phosphorylation and its specific patterns can not only alter the threshold concentrations for phase-separation (Fig.3A and Supplementary Fig. S4) but also serve as effective modulator of intra-condensate dynamics (Fig.3C and D).

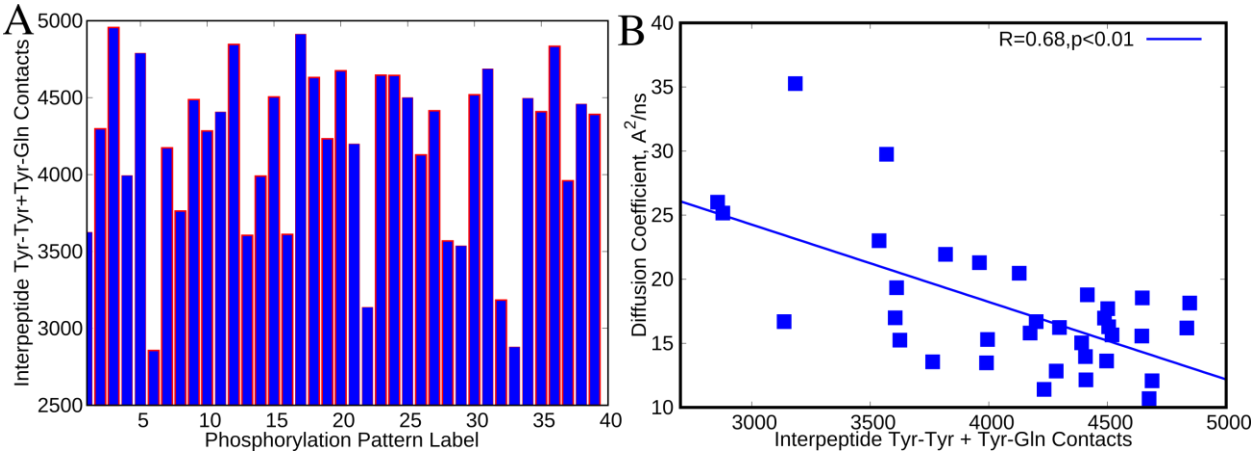

Figure 4: Phosphorylation patterns influence inter-peptide contact probability. A) Inter-chain contacts involving Tyrosine and Glutamine residues, for PLD sequences with different modification patterns with 50% of phosphosites modified (P_{frac} = 0.5). B) Intracluster diffusion coefficients show a negative correlation with inter-peptide contacts involving Tyr and Gln. We observe a 4-fold variability in intra-cluster dynamics, for different modification patterns.

Phosphorylation pattern, and not just net-charge of the PLD, influences intracluster dynamics

Our results so far demonstrate the efficacy of phosphorylation as a tunable handle for intra-cluster dynamics, with higher modification fractions resulting in liquid-like clusters. However, even for the same modification fraction, P_{frac}, we observe variability in inter-chain contacts and diffusion constants (Fig 2 and 3) for different phosphorylation patterns. To further understand how

the positioning of phosphorylated phosphosites could influence the behavior of the condensates, we performed simulations with 40-different phosphorylation patterns, each with P_{frac} = 0.5. Strikingly, for the 40 randomly generated phosphorylation patterns, we observe a significant variation in the total inter-peptide contacts within the cluster. As evident from Fig. 4A, we observe a 2-fold variability in inter-molecular contacts between different phosphorylation patterns despite the net charge of the domain due to the modification being the same. This variability in inter-molecular contacts also gives rise to a 2-fold variation in diffusion coefficients of PLD peptides within the clusters (Fig.4B). This broad distribution in contact densities indicates that the interaction network and intra-cluster dynamics depends not just on the net negative charge of the domain but also on the location of phosphosites.

This pattern-dependence of intra-cluster dynamics gives rise to an interesting evolutionary question. Are phosphosite locations non-random and correlated with the location of amyloid hotspots in the FUS prion-like domain? To address this question, we first plot the amyloidigenic propensity of FUS using the ZipperDB algorithm[45] which computes the compatibility of hexapeptide stretches within protein sequences with the amyloid cross-beta architecture. Interestingly, the amyloidigenicity profile for the unmodified human FUS PLD sequences shows 8 stretches (labelled C1-C8) with ZipperDB energy lower than the reference template, the GNQQNY peptide (Fig.5A). The fully phosphorylated sequence (Fig.5B), with S/T → E shows a complete abrogation of amyloid propensity of the PLD.

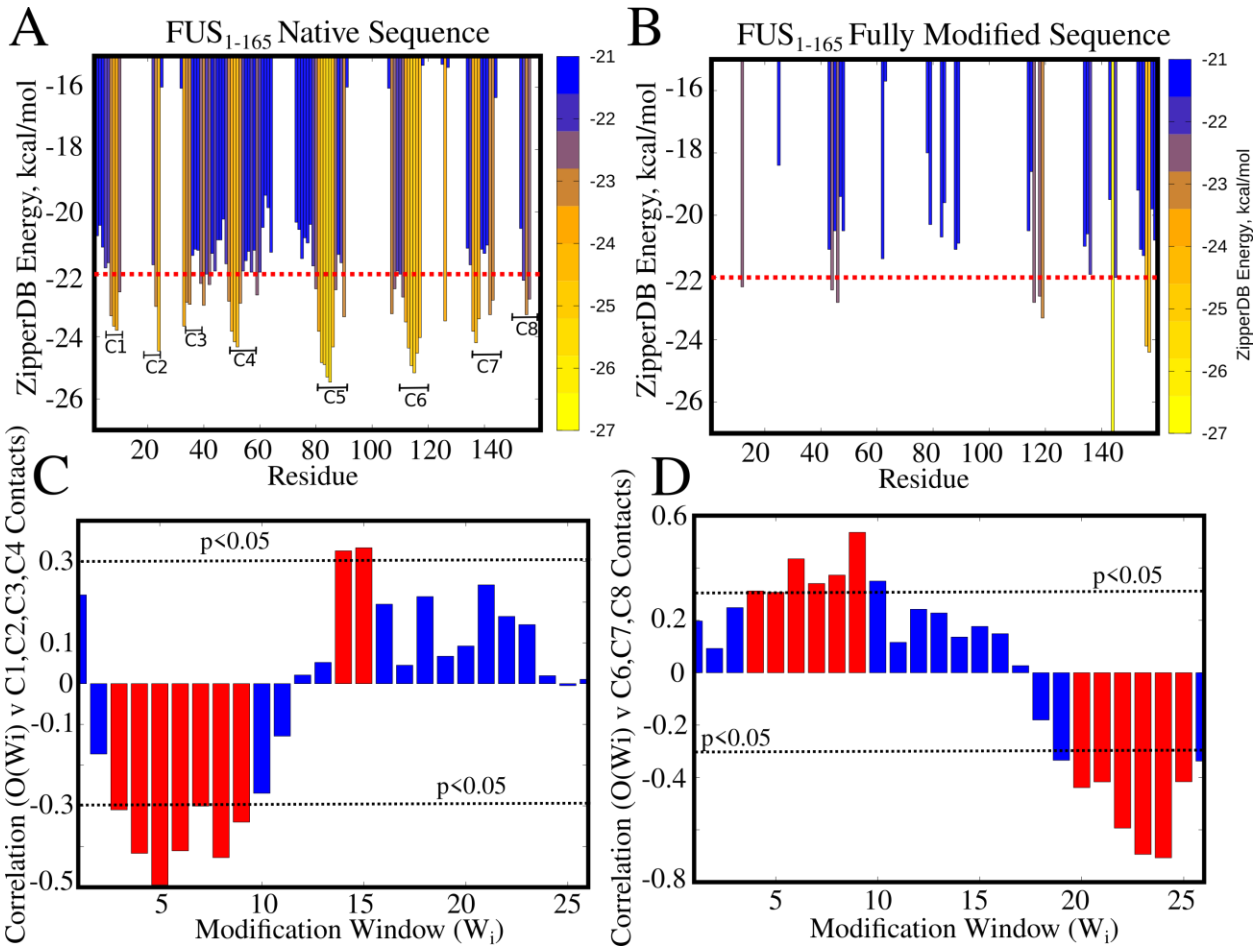

Figure 5: Phosphorylation sites reduce likelihood of amyloidigenic contacts locally. Amyloidigenicity profiles for A) unmodified human FUS PLD, and B) fully phosphorylated FUS PLD sequences. The ZipperDB energy (kcal/mol) indicates the compatibility of a hexapeptide stretch within the protein to the steric-zipper amyloid architecture. Values lower than -22 kcal/mol indicate that the hexapeptide stretch is compatible with the cross-beta structure. C) and D) Phosphorylation patterns are described by 26 overlapping modification windows of 5 consecutive phosphosites -- W_i. For e.g, the modification window W_1 comprises of phosphosites at S3,T7,T11,T19,S26 whereas the second modification window W_2 comprises of phosphosites T7,T11,T19,S26,S30. The occupancy of any modification window $O(W_1)$ to $O(W_{25})$, for any phosphorylation pattern, is the fraction of residues in the window that are modified. $O(W_i)$ can , therefore, take values between 0 and 1. Every phosphorylation pattern can thus be defined as a string of occupancy values [$O(W_1)$, $O(W_2)$…..$O(W_{25})$]. The extent of correlation between different occupancies ($O(W_1)$ to $O(W_{25})$) and the corresponding to the sum of amyloid core contacts involving the C1,C2,C3,C4 regions is shown in (C) and C6,C7,C8 in (D). The dotted line respresents the point beyond which the correlations are statistically significant..

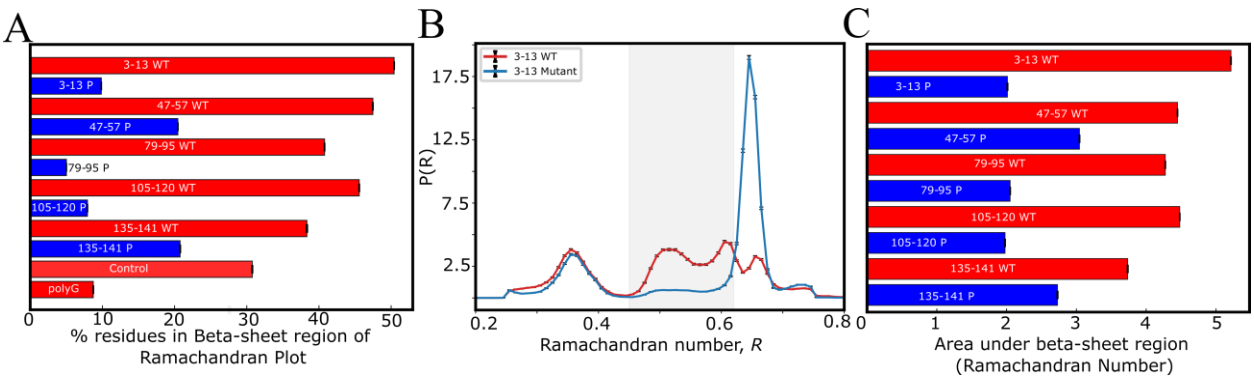

Fig.6 Beta-sheet propensity of amyloid core-derived peptides in atomistic simulations. A) Proportion of residues in the β-sheet region of the Ramachandran plot for self-assembly simulations with 50 copies of peptides corresponding to different amyloid core regions (C1-C8 in Fig.5). B) Area under the curve in the Ramachandran number plots. The Ramachandran number, $R(\varphi,\psi) = (\varphi+\psi+2\pi)/4\pi$. The red bars correspond to simulations with native peptide sequence (WT) while the blue bars correspond to phosphomimetic variants of the segment, with phosphosite residues of the WT modified to Glutamic acid. Introduction of a negative charge at the phosphosite location via glutamic acid substitution results in a significant decrease in the accessibility to the β-sheet region of the Ramachandran plot.

We further investigate why different phosphorylation patterns result in a variability in inter-chain contacts and diffusion coefficients, despite the sequences harboring the same net charge. In other words, we test the following hypothesis – if the effect of phosphorylation were merely net-charge driven, any phosphorylation pattern would result in a reduction of contacts involving all 8 amyloid cores (C1 to C8 in Fig.5A) to a similar extent. To address this question, we define a quantity – occupancy of modification window -- O(Wi) – that describes different phosphorylation patterns. Here, phosphorylation patterns are described by 26 overlapping modification windows of 5 consecutive phosphosites. For instance, the modification window W_1 comprises of phosphosites at S3,T7,T11,T19,S26 whereas the second modification window W_2 comprises of phosphosites T7,T11,T19,S26,S30. Similarly, the W_{25} is defined by phosphosites S129,S131,S135,S142,S148. The occupancy of any modification window $O(W_1)$ to $O(W_{25})$, for any phosphorylation pattern, is the fraction of residues in the window that are modified. $O(W_i)$ can , therefore, take values between 0 and 1. Every phosphorylation pattern can thus be defined as a string of occupancy values $[O(W_1), O(W_2)\ldots..O(W_{25})]$. We first compute the correlation between the occupancy of any given window (for 40 different sequences with Pfrac = 0.5) and the amyloid core contacts involving different amyloid cores C1-C8. For instance, in Supplementary Fig.S5A, we show a scatter plot for occupancy of W25 (S129,S131,S135,S142,S148) versus amyloid core contacts involving C6, C7, C8 (region 115-150 in Fig.5A). As evident from Fig. S5A, we observe a statistically significant negative correlation between occupancies in this modification window

and the amyloid core contacts involving C6, C7 and C8 cores. On the other hand, the occupancy of W1 shows no such correlation (Fig. S5B). In Fig.5C and D, we plot the extent of correlation between different occupancies ($O(W_1)$ to $O(W_{25})$) and the sum of corresponding amyloid core contacts involving C1,C2,C3,C4 (Fig.5C) and C6,C7,C8 (Fig.5D).

Interestingly, an increased occupancy of modification windows W_1 to W_{10} results in a statistically significant negative correlation with amyloid core contacts involving C2,C3 and C4. For windows labeled W11 to W24 we either observe a weak positive or statistically insignificant correlation for C2,C3,C4 contacts. In other words, to reduce the density of contacts involving C2,C3,C4, the modification patterns must enrich phosphosites that are localized in the N-terminal region of the protein. Similarly, to reduce the likelihood of amyloid core contacts involving the C6, C7 and C8 regions, the phosphorylation patterns must involve residues that comprise modification windows W_{20} to W_{25}, i.e the region between residues 110-140 of the protein. In fact, for patterns which have low occupancies in W20 to W25 and higher occupancies for W4 to W10, we observe an increase in C6, C7, C8 contacts, as seen from a statistically significant positive correlation for these regions in Fig.5D. Our results suggest that an effective phosphorylation pattern must, therefore, include modification sites that are in the vicinity of each potential amyloid core (C1 to C8) in the $FUS_{1\text{-}165}$ sequence.Our coarse-grained simulations reveal a strongly local, position specific effect of phosphorylation.

While the coarse-grained simulations can capture the effect of phosphomimetic substitutions on inter-peptide contacts, the coarse-grained model cannot capture secondary structural transitions. We therefore performed all-atom molecular dynamics simulations with different amyloid-core segments from $FUS_{1\text{-}165}$ and studied the difference in secondary structural propensity of various amyloid core peptides (Supplementary Table S4) – i) 3-13 (Core C1), ii) 47-57 (Core C4) iii) 79-95 (Core C5) iv) 105-120 (Core C6) v) 135-141 (Core C7) – in the presence and absence of phosphomimetic substitutions. In order to study the local effect of phosphorylation on the amyloid core contacts, we introduce a negative charge via a Glutamic-acid substitution at the phosphosite location (blue bars with labels tagged P in Figure 6). Using metadynamics simulations we drive the self-assembly of peptides into large clusters at simulation timescale (100 ns). We then analyze the secondary structural content of the system by computing the proportion of all residues in the system in the beta-sheet region of the Ramachandran plot (across 50 copies of the peptide in the simulation box). Strikingly, while the β-sheet content for the wild-type

peptides can be as high as 50%, introduction of phosphomimetic substitutions results in a reduction of β-sheet content by more than half, in all the peptides under study. The β-sheet content for phosphomimic sequences (tagged P) approaches that of the polyG sequence which has natively low propensity for β-sheets. We further analyzed the secondary structural propensity using the Ramachandran number[46] – a secondary structural order parameter that collapses the 2-dimensional information from the Ramachandran plot (Eqn. 4). In Fig.6B and Supplementary Fig. S6 we show the Ramachandran number plots for various amyloid core peptides and their phosphomimetic counterparts.

$$R(\varphi,\psi) = (\varphi+\psi+2\pi)/4\,\pi \qquad (4)$$

The Ramachandran number for any residue in equation 4 ranges from 0 to 1, with the combination of φ,ψ angles corresponding to the β-sheet region resulting in R(φ,ψ) values between 0.45 to 0.65 (shaded region in Fig. 6B,C). As evident from the Ramachandran number plot in Supplementary Fig. S6, the area under the β-sheet region of the Ramachandran number curve goes down for phosphomimic substitutions, for all peptides under study (Fig. 6B,C and Supplementary Fig.S6). These results establish that introduction of a negatively charged phosphomimetic substitution in the vicinity of the amyloidogenic region results in a reduced accesibility to the β-sheet of the Ramachandran plot. These results indicate that phosphorylation can be an effective local checkpoints against inter-peptide β-sheet formation, a signature of the amyloid-like state.

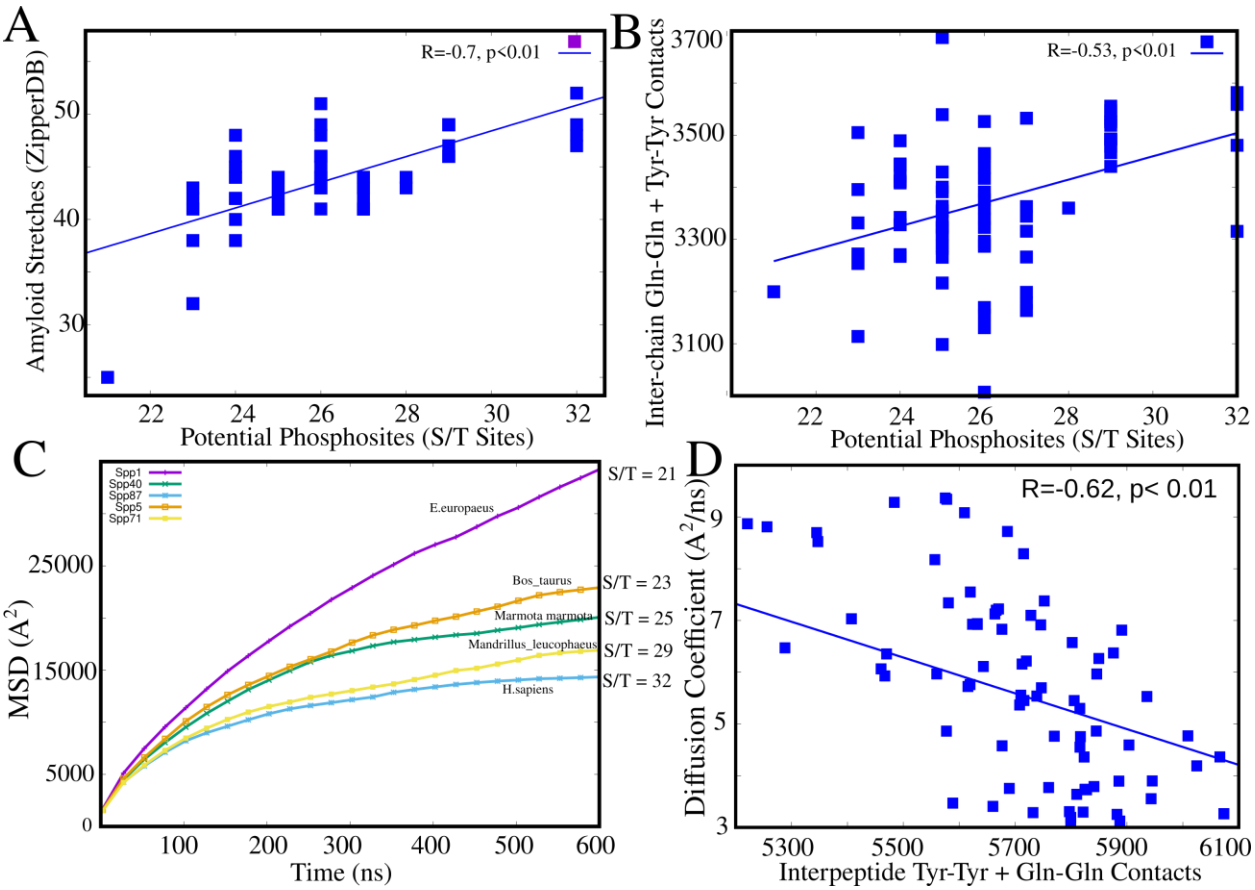

Figure 7: Evolutionary enrichment of phosphosites to ensure liquidity of condensates. A) Correlation between the total number of cross-beta amyloid-compatible stretches in a mammalian FUS PLD sequence and the total number of potential phosphosites in the same sequence. A statistically significant correlation of 0.7 was observed ($p<0.01$). B) Correlation between the number of phosphosites in any mammalian sequence, and the total number of sticky interactions (involving Tyr and Gln) within the self assembled cluster (computed from simulations). Each datapoint corresponds to a different mammalian FUS PLD sequence. C) Mean square displacement profiles for different representative mammalians sequences with different number of potential phosphosites. D) Mammalian sequences that are more prone to intra-cluster Q-Q,Y-Y contacts show less dynamic behavior in simulations.

Evolution selects phosphosites in the vicinity of FUS amyloidigenic regions

PLD sequences with the same modification fraction but different phosphosites can exhibit variability in inter-protein contacts as well as intra-cluster dynamics (Figs.3 - 5). The local effect of phosphorylation, as opposed to a net-charge effect gives rise to a crucial question. Could phosphosite loci, have evolved to reduce the overall amyloidigenic propensity (across different amyloid cores) in the PLD of FUS proteins?

To test this hypothesis, we investigate the amyloidigenic propensity and the corresponding phosphosites in 85 different mammalian FUS PLD sequences (Fig 7A). Interestingly, we observe

a strong correlation between the native amyloidigenic propensity and the potential number of phosphosites in a mammalian FUS PLD sequence. This result suggests that PLD sequences that are inherently more prone to solidification via amyloid-like interactions more likely require phosphosites to prevent possible aberrant transitions. We further simulate these 85-mammalian FUS PLD sequences using the coarse grained model and observe a statistically significant correlation between sticky interactions (Y-Y and Q-Q) within the cluster and the potential phosphosites in the sequence (Fig.7B). Importantly, different mammalian PLD sequences also show dramatically different intra-cluster dynamics, with the native primate PLD sequences which harbor the most number of phosphosites showing the slowest intracluster diffusion (Fig.7C). PLDs of mammalian sequences with fewer number of phosphosites were more likely to assemble into liquid-like clusters. Consistent with this hypothesis, sequences which are more prone to forming Q-Q and Y-Y contacts also exhibit slower intra-cluster dynamics in our simulations (Fig. 7D).

Since amyloid-forming regions increase the propensity of protein-protein interactions in PLD sequences, phosphorylation sites may serve as checkpoints against liquid-solid transition via amyloid-prone regions in low complexity domains of these proteins. To test this hypothesis, we compared the number of amyloid-prone regions in mammalian PLD sequences with 100 artificial comparison protein sequences that we generated to evolve neutrally. Briefly, we simulated neutral protein sequence evolution using the codon composition that matches PLD sequences, and employed realistic divergence times of mammalian FUS sequence (Figure 8A, see Methods for details). We then evaluated the number of amyloid-forming residues (ZipperDB energy < -22 kcal/mol) in these neutrally-evolved sequences and compared them with those found in mammalian PLD sequences. As shown in Figure. 8B, the number of such residues per 100 amino acids were ~ 19.38 ± 2.91 in mammalian sequences which was significantly higher than the number of amyloid-forming residues in control neutrally-evolved sequences (=3.15 ± 1.62; $p < 10^{-16}$; Two-sided Kolmogorov-Smirnov test). This shows that evolution has significantly enriched the mammalian PLD sequences in amyloid-forming regions compared to neutrally evolving control sequences.

Next, we investigated whether phosphorylation sites have evolved under selection to minimize protein aggregation via amyloid-formation. To that end, we compared the distributions of the distances of phosphosites from amyloid forming regions in mammalian sequences and the simulated sequences that had evolved neutrally (see Methods for details). These distances were

indeed significantly shorter in mammalian PLD sequences compared to neutrally evolved ones (Figure 8B, $p < 10^{-16}$; Wilcoxon rank-sum test). Furthermore, the local sequence environment close to the amyloid-forming regions in mammalian PLD sequences were significantly enriched in dipeptides containing serine compared to neutrally evolved sequences making them suitable kinase motifs (Supplementary Figure S7). Together with simulations results presented in Fig.5 these observations show that evolution placed phosphorylation sites near amyloid-forming regions likely as checkpoints to minimize amyloid formation and liquid-to-solid phase transition.

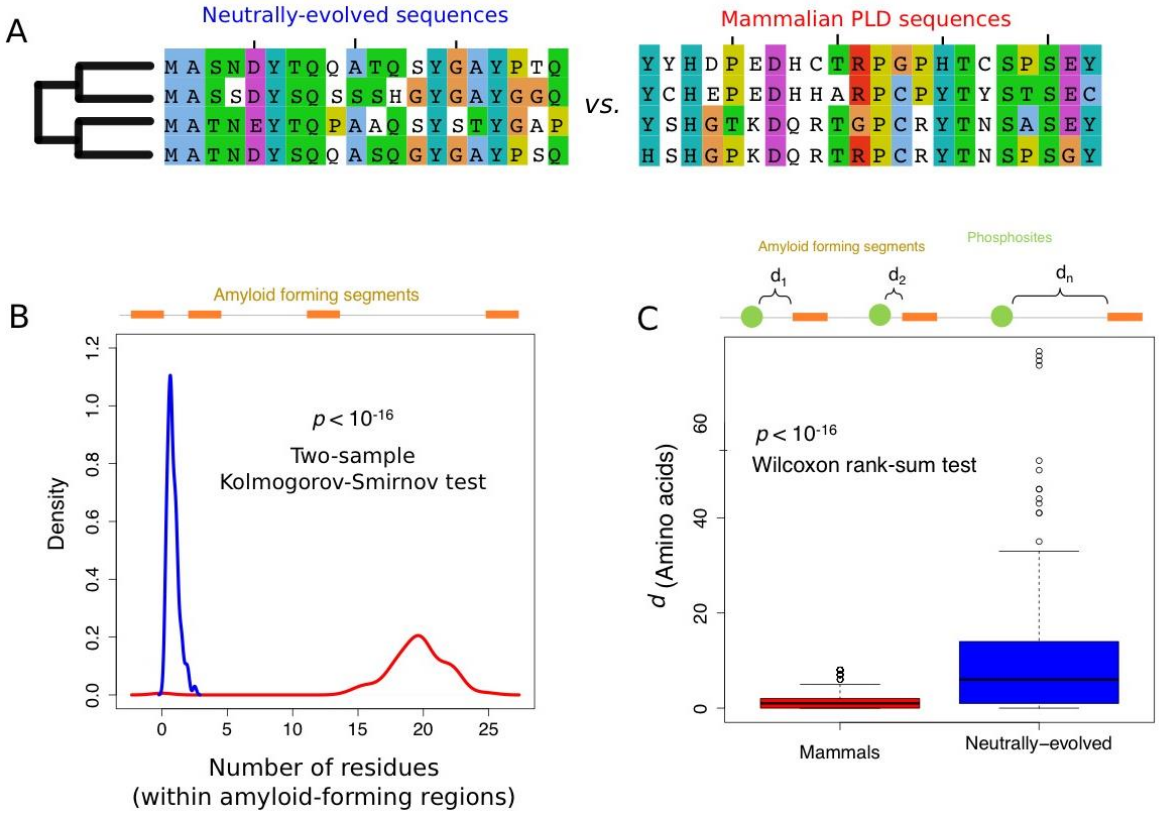

Figure 8. The number of amyloid-forming regions and their proximity to potential phosphorylation sites have evolved under positive selection. A) We compared the number of amyloid forming regions and the distance of phosphosites to such regions in mammalian PLD sequences, and sequences that had evolved under neutral evolution (see Methods for details of simulations). B) The density of the number of amyloid forming residues (ZipperDB energy < -22 kcal/mol) in mammaoian PLD sequences (shown in blue), and neutrally-evolved sequences (shown in red). C) The distance between potential phosphosites and amyloid forming residues in mammaoian PLD sequences (shown in blue), and neutrally-evolved sequences (shown in red). We predicted the phosphorylation sites in neutrally-evolved sequences using NetPhos v3.0 server.

Discussion

The assembly of multivalent biomolecules into dynamic compartments is exploited by living cells as a means of spatio-temporal organization[47] to optimize various biochemical processes Among the various motifs that have emerged to achieve LLPS at physiologically relevant conditions are intrinsically disordered regions (IDRs) in proteins and prion-like domains[10,13,20]. While being efficient promoters of phase-separation, these short linear motifs in IDRs are also often extremely prone to aberrant, irreversible aggregation into amyloid-like structures.[48] The ability of proteins harboring PLDs to switch between different interaction modes could help them access diverse states including the liquid-like and amyloid-like configurations. While full-length FUS readily assembles into dynamic liquid-like droplets in vitro, these droplets undergo structural (and dynamic) transition to solid-like aggregates upon prolonged incubation[14]. Living systems, therefore, operate at the edges of biomolecular phase-transitions, with small perturbations often resulting in a dramatically altered state of a system. Studying the mechanisms that allow cells to exploit the inherent self-assembling propensity of IDRs while guarding against aberrant phase transitions can help shed light on biomolecular function and cellular evolution.

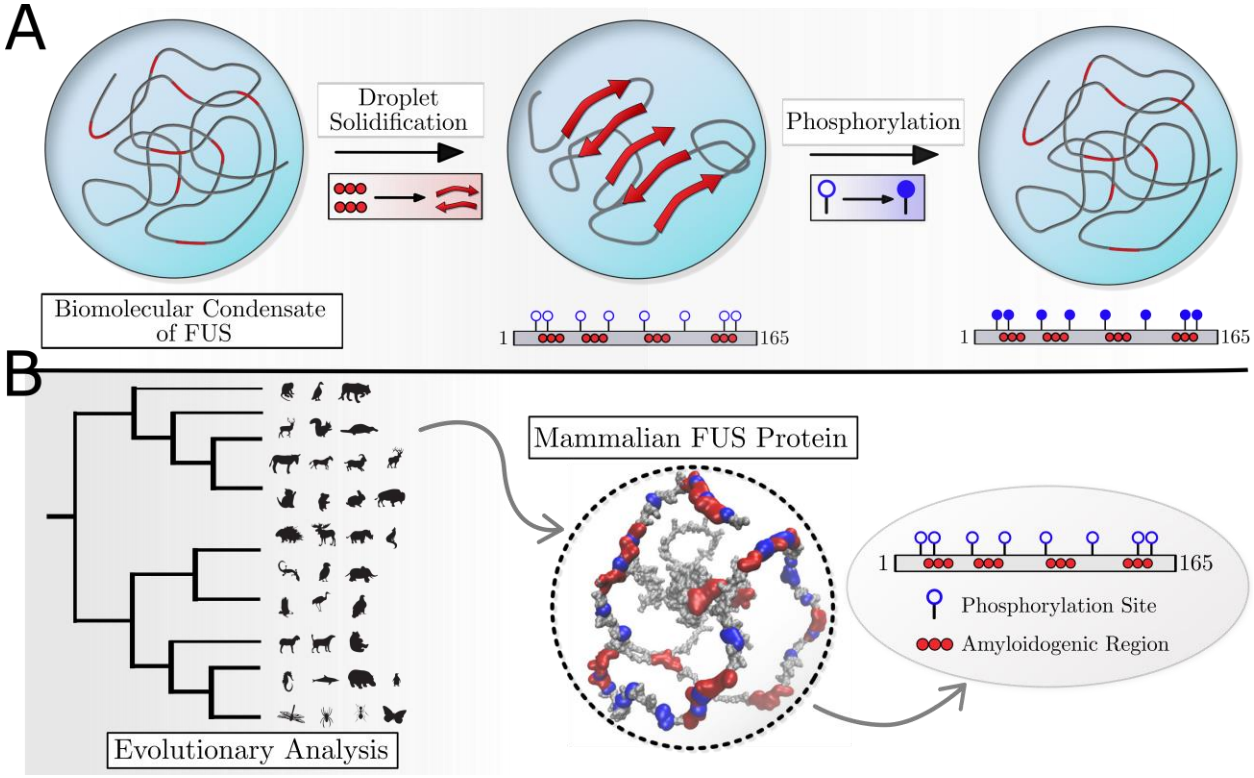

Figure 9. Graphical summary of the study. A) Coarse-grained simulations show that phosphorylation results in a decrease in sticky Tyrosine and Glutamine contacts that result in a more dynamic intra-cluster

environment. B) Evolutionary bioinformatics analysis and coarse-grained simulations with 85 mammalian FUS PLD sequences reveals a strong correlation between the number of phosphorylation sites (purple beads in the ball and stick representation) and the amyloidogenic propensity (red beads in the ball and stick representation) of the native sequence. Comparison with neutrally evolved sequences reveals that mammalian sequences localize phosphosites in the vicinity of amyloid prone regions.

In this work, we use a coarse-grained computational model and evolutionary analysis to explore the role of phosphorylation in controlling the phase-separation of FUS assemblies. Notably, we demonstrate how the interaction networks stabilizing the self-assembled state, and the intra-cluster dynamics of proteins could be influenced by phosphorylation at 31 potential phosphosites (S/T residues) in human FUS (Supplementary Table. S1 and S2). While unmodified assemblies of full-length human FUS protein showed an equal likelihood of both homodomain (PLD-PLD interactions) and heterodomain (PLD-RBD interactions stabilized by Tyr-Arg contacts interactions, a systematic increase in extent of phosphorylation resulted in an increased likelihood of PLD-RBD interactions (Fig. 2A). This switch in interaction network is an outcome of sparser PLD-PLD contacts and reduced 'sticky' Tyr-Tyr/Gln-Gln/Tyr-Gln interactions. This shift in interaction networks was found to be an outcome of perturbations in PLD-PLD interactions, while PLD-RBD interactions remain unaffected (Fig.2). Therefore, phosphorylation selectively reduces the valency of the FUS PLD with respect to other PLDs while the effective valency of PLD-RBD interactions remains the same (Fig.2). A direct outcome of sparser sticky interactions was observed in a systematic increase in diffusion coefficients upon increase in extent of phosphorylation (Fig. 3C and D). This increase in diffusion coefficients suggests that phosphorylation ensures liquidity of the intra-droplet environment in an otherwise viscous intracluster environment (Fig. 9A).

Phosphorylation influences droplet behavior in not just a net-charge dependent manner but also a position-specific, pattern-dependent manner (Fig. 5). We found that the origin of this pattern-dependent variability lies in the uniform distribution of "amyloid-core" patches in the protein (Fig. 5A). Modifications clustered in one part of the protein were found to only influence amyloid-like contacts in the vicinity of the phosphosites, leaving amyloid-like contacts in other parts of the protein largely unaffected (Fig.5C and D). The ability of phosphomimetic substitutions in abrogating amyloidogenicity is further supported by atomistic molecular dynamics simulations which show an abrogation of beta-sheet propensity in phosphomimic counterparts of amyloid core peptides (Fig. 6).

Stochasticity in phosphorylation patterns has been previously reported in studies where only a

small fraction of FUS shows complete phosphorylation [8, 21]. The nature of physical stress has also been shown an impact on phosphorylation pattern, with Ser-42 phosphorylation being a more prevalent modification in response to IR damage, while UV radiation resulted in an increase in Ser-26 modification[49,50]. Our simulations further support these findings and suggest that this pattern-dependence could be exploited by cells to differentially regulate droplet behavior. Cells could selectively phosphorylate only a small fraction of critical phosphorylation sites so as to ensure dynamicity of droplets while retaining the ability to phase separate. Sensitivity to the extent and pattern of phosphorylation therefore offers cells granular control over condensate assembly, disassembly and dynamics.

To efficiently abrogate amyloidigenicity, these phosphosites must therefore spatially correlate with the location of amyloid-prone regions in the PLD sequence. In order to test this hypothesis, we studied 85 mammalian sequences for their amyloid propensity profiles as well as inter-peptide contacts using Langevin dynamics simulations. Dasmeh et al[19] have previously established that the PLD of FUS is the region of the protein that shows the highest degree of sequence entropy in the alignment, with $S \rightarrow G$ and $G \rightarrow S$ being the most abundant substitutions in the 85 mammalian PLD sequences. $G \rightarrow S$ transitions resulting in phosphosites is 3-fold more likely in primate FUS PLD sequence as compared to their other mammalian counterparts. Primate sequences which harbor the greatest number of phosphosites also result in clusters with a greater number of Y/Q contacts (Fig. 6B). In general, the mammalian FUS sequences that result in less dynamic assemblies were also more likely to contain greater number of potential phosphosites (Fig.6A, C, D). Positive selection for phosphosites in primate FUS PLD sequences could therefore be an evolutionary mechanism to ensure the dynamicity of structures prone to amyloid formation (Fig.6C). Therefore, we hypothesized that amyloid-prone sequences get utilized by cells to promote protein clustering at lower threshold concentrations while the potential drawback of this mechanism - aberrant transitions to irreversible solid-like structures - are prevented by phosphorylating residues in the vicinity of these amyloid cores. This is further bolstered by protein sequence evolution studies which suggest that mammalian FUS sequences are indeed significantly more likely to harbor amyloidigenic sites compared to neutrally evolved sequences with same codon frequencies as mammalian FUS sequences (Fig.7 and Supplementary Fig.S7). Further, the distance between amyloidigenic sites and the nearest phosphosite was also significantly shorter in mammalian FUS sequences, as compared to the neutrally evolved counterparts with no selection

pressure. Evolution, therefore, uses phosphorylaton as a switch that could help cells toggle the state of the protein-rich cluster, by shifting phase boundaries as well as intra-cluster dynamics of proteins (Fig. 9B). This could allow cells to exploit aggregation-prone stretches to promote phase-separation and biomolecular condensation while safeguarding against the detrimental effects of amyloidosis .

Acknowledgement. The authors would like to thank Junlang Liu, Eugene Serebryany, David Thorn and Amir Bitran for their suggestions and valuable discussions.

Declaration of Interests. The authors declare that they have no competing interests.

Author Contribution. SR, PD and ES were involved in the conceptualization of the work. SR, PD and ES wrote the paper. SR designed and performed the coarse-grained simulations. PD setup and performed the bioinformatics study. SF performed the atomistic simulations and analyzed the all-atom simulation data.

References

1. Banani, S. F., Lee, H. O., Hyman, A. A. & Rosen, M. K. *Biomolecular condensates: Organizers of cellular biochemistry*.
2. Boeynaems, S. *et al.* Spontaneous driving forces give rise to protein–RNA condensates with coexisting phases and complex material properties. *Proc Natl Acad Sci U S A* **116**, 7889–7898 (2019).
3. Brangwynne, C. P., Mitchison, T. J. & Hyman, A. A. Active liquid-like behavior of nucleoli determines their size and shape in Xenopus laevis oocytes. *Proceedings of the National Academy of Sciences* **108**, 4334 LP – 4339 (2011).
4. Brangwynne, C. P. Phase transitions and size scaling of membrane-less organelles. *Journal of Cell Biology* **203**, 875–881 (2013).
5. Protter, D. S. W. & Parker, R. Principles and Properties of Stress Granules. *Trends Cell Biol* **26**, 668–679 (2017).
6. Harmon, T. S., Holehouse, A. S., Rosen, M. K. & Pappu, R. v. Intrinsically disordered linkers determine the interplay between phase separation and gelation in multivalent proteins. *Elife* **6**, e30294 (2017).
7. Li, P. *et al.* Phase transitions in the assembly of multivalent signalling proteins. *Nature*

483, 336–340 (2012).

8. Gomes, E. & Shorter, J. The molecular language of membraneless organelles. *Journal of Biological Chemistry* **294**, 7115–7127 (2019).
9. Wang, J. T. *et al.* Regulation of RNA granule dynamics by phosphorylation of serine-rich, intrinsically disordered proteins in C. elegans. *Elife* **3**, e04591 (2014).
10. Lin, Y., Currie, S. L. & Rosen, M. K. Intrinsically disordered sequences enable modulation of protein phase separation through distributed tyrosine motifs. *Journal of Biological Chemistry* **292**, 19110–19120 (2017).
11. Wang, J. *et al.* A Molecular Grammar Governing the Driving Forces for Phase Separation of Prion-like RNA Binding Proteins. *Cell* **174**, 688—-699.e16 (2018).
12. Shewmaker, F., Wickner, R. B. & Tycko, R. Amyloid of the prion domain of Sup35p has an in-register parallel β-sheet structure. *Proceedings of the National Academy of Sciences* **103**, 19754–19759 (2006).
13. Gomes, E. & Shorter, J. The molecular language of membraneless organelles. *Journal of Biological Chemistry* **294**, 7115–7127 (2019).
14. Murakami, T. *et al.* ALS/FTD Mutation-Induced Phase Transition of FUS Liquid Droplets and Reversible Hydrogels into Irreversible Hydrogels Impairs RNP Granule Function. *Neuron* **88**, 678–690 (2015).
15. Lin, Y., Protter, D. S. W., Rosen, M. K. & Parker, R. Formation and Maturation of Phase-Separated Liquid Droplets by RNA-Binding Proteins. *Mol Cell* **60**, 208–219 (2015).
16. Hofweber, M. & Dormann, D. Friend or foe-Post-translational modifications as regulators of phase separation and RNP granule dynamics. *Journal of Biological Chemistry* vol. 294 7137–7150 Preprint at https://doi.org/10.1074/jbc.TM118.001189 (2019).
17. Owen, I. & Shewmaker, F. The Role of Post-Translational Modifications in the Phase Transitions of Intrinsically Disordered Proteins. *Int J Mol Sci* **20**, (2019).
18. Monahan, Z. *et al.* Phosphorylation of the FUS low-complexity domain disrupts phase separation, aggregation, and toxicity. *EMBO J* **36**, 2951–2967 (2017).
19. Dasmeh, P. & Wagner, A. Natural Selection on the Phase-Separation Properties of FUS during 160 My of Mammalian Evolution. *Mol Biol Evol* **38**, 940–951 (2020).
20. Dignon Gregory L. AND Zheng, W. A. N. D. K. Y. C. A. N. D. B. R. B. A. N. D. M. J. Sequence determinants of protein phase behavior from a coarse-grained model. *PLoS Comput Biol* **14**, 1–23 (2018).
21. Ashbaugh, H. S. & Hatch, H. W. Natively Unfolded Protein Stability as a Coil-to-Globule Transition in Charge/Hydropathy Space. *J Am Chem Soc* **130**, 9536–9542 (2008).
22. Perdikari, T. M. *et al.* A predictive coarse-grained model for position-specific effects of post-translational modifications. *Biophys J* **120**, 1187–1197 (2021).
23. Dignon, G. L., Zheng, W., Best, R. B., Kim, Y. C. & Mittal, J. Relation between single-molecule properties and phase behavior of intrinsically disordered proteins. *Proc Natl Acad Sci U S A* **115**, 9929–9934 (2018).
24. Anoop, A. *et al.* Elucidating the role of disulfide bond on amyloid formation and fibril reversibility of somatostatin-14: Relevance to its storage and secretion. *Journal of Biological Chemistry* **289**, 16884–16903 (2014).
25. Ranganathan, S., Maji, S. K. & Padinhateeri, R. Defining a Physical Basis for Diversity in Protein Self-Assemblies Using a Minimal Model. *J Am Chem Soc* **138**, 13911–13922

(2016).
26. Ranganathan, S. & Shakhnovich, E. The physics of liquid-to-solid transitions in multi-domain protein condensates. *Biophys J* (2022) doi:https://doi.org/10.1016/j.bpj.2022.06.013.
27. Ranganathan, S. & Shakhnovich, E. I. Dynamic metastable long-living droplets formed by sticker-spacer proteins. *Elife* (2020) doi:10.7554/eLife.56159.
28. Holehouse, A. S., Ginell, G. M., Griffith, D. & Böke, E. Clustering of Aromatic Residues in Prion-like Domains Can Tune the Formation, State, and Organization of Biomolecular Condensates. *Biochemistry* **60**, 3566–3581 (2021).
29. Benayad, Z., von Bülow, S., Stelzl, L. S. & Hummer, G. Simulation of FUS Protein Condensates with an Adapted Coarse-Grained Model. *J Chem Theory Comput* **17**, 525–537 (2021).
30. Bieler, N. S., Knowles, T. P. J., Frenkel, D. & Vácha, R. Connecting macroscopic observables and microscopic assembly events in amyloid formation using coarse grained simulations. *PLoS Comput Biol* **8**, e1002692 (2012).
31. Šarić, A., Chebaro, Y. C., Knowles, T. P. J. & Frenkel, D. Crucial role of nonspecific interactions in amyloid nucleation. *Proceedings of the National Academy of Sciences* **111**, 17869–17874 (2014).
32. Garaizar, A. *et al.* Aging can transform single-component protein condensates into multiphase architectures. (2022) doi:10.1073/pnas.
33. Dignon, G. L., Zheng, W., Kim, Y. C., Best, R. B. & Mittal, J. Sequence determinants of protein phase behavior from a coarse-grained model. *PLoS Comput Biol* (2018) doi:10.1371/journal.pcbi.1005941.
34. Plimpton, S. Fast Parallel Algorithms for Short-Range Molecular Dynamics. *J Comput Phys* **117**, 1–19 (1995).
35. Laio, A. & Gervasio, F. L. Metadynamics: a method to simulate rare events and reconstruct the free energy in biophysics, chemistry and material science. *Reports on Progress in Physics* **71**, 126601 (2008).
36. Phillips, J. C. *et al.* Scalable molecular dynamics with NAMD. *J Comput Chem* **26**, 1781–1802 (2005).
37. Huang, J. *et al.* CHARMM36m: an improved force field for folded and intrinsically disordered proteins. *Nat Methods* **14**, 71–73 (2017).
38. Yang, Z. PAML: a program package for phylogenetic analysis by maximum likelihood. *Bioinformatics* **13**, 555–556 (1997).
39. Yang, Z. PAML 4: Phylogenetic Analysis by Maximum Likelihood. *Mol Biol Evol* **24**, 1586–1591 (2007).
40. Hedges, S. B., Dudley, J. & Kumar, S. TimeTree: a public knowledge-base of divergence times among organisms. *Bioinformatics* **22**, 2971–2972 (2006).
41. Yang, Z. & Nielsen, R. Codon-Substitution Models for Detecting Molecular Adaptation at Individual Sites Along Specific Lineages. *Mol Biol Evol* **19**, 908–917 (2002).
42. Dasmeh, P. & Wagner, A. Natural Selection on the Phase-Separation Properties of FUS during 160 My of Mammalian Evolution. *Mol Biol Evol* **38**, 940–951 (2021).
43. Patel, A. *et al.* A Liquid-to-Solid Phase Transition of the ALS Protein FUS Accelerated by Disease Mutation. *Cell* **162**, 1066–1077 (2015).

44. Wang, J. *et al.* A Molecular Grammar Governing the Driving Forces for Phase Separation of Prion-like RNA Binding Proteins. *Cell* **174**, 688-699.e16 (2018).
45. Thompson, M. J. *et al.* The 3D profile method for identifying fibril-forming segments of proteins. *Proc Natl Acad Sci U S A* **103**, 4074–8 (2006).
46. Mannige, R. v, Kundu, J. & Whitelam, S. The Ramachandran Number: An Order Parameter for Protein Geometry. *PLoS One* **11**, e0160023- (2016).
47. Banani, S. F., Lee, H. O., Hyman, A. A. & Rosen, M. K. Biomolecular condensates: organizers of cellular biochemistry. *Nat Rev Mol Cell Biol* **18**, 285 (2017).
48. Patel, A. *et al.* A Liquid-to-Solid Phase Transition of the ALS Protein FUS Accelerated by Disease Mutation. *Cell* (2015).
49. Rhoads, S. N. *et al.* The prionlike domain of FUS is multiphosphorylated following DNA damage without altering nuclear localization. *Mol Biol Cell* **29**, 1786–1797 (2018).
50. Gardiner, M., Toth, R., Vandermoere, F., Morrice, N. A. & Rouse, J. Identification and characterization of FUS/TLS as a new target of ATM. *Biochemical Journal* **415**, 297–307 (2008).